

**Magnetoelectric effect in doped magnetic ferroelectrics**O. G. Udalov<sup>1,2</sup> and I. S. Beloborodov<sup>1</sup><sup>1</sup>*Department of Physics and Astronomy, California State University Northridge, Northridge, California 91330, USA*<sup>2</sup>*Institute for Physics of Microstructures, Russian Academy of Science, Nizhny Novgorod 603950, Russia*

(Received 24 May 2017; published 19 July 2017)

We propose a model of magnetoelectric effect in doped magnetic ferroelectrics. This magnetoelectric effect does not involve the spin-orbit coupling and is based purely on the Coulomb interaction. We calculate magnetic phase diagram of doped magnetic ferroelectrics. We show that magnetoelectric coupling is pronounced only for ferroelectrics with low dielectric constant. We find that magnetoelectric coupling leads to modification of magnetization temperature dependence in the vicinity of the ferroelectric phase transition. A peak of magnetization appears. We find that magnetization of doped magnetic ferroelectrics strongly depends on the applied electric field.

DOI: [10.1103/PhysRevB.96.024204](https://doi.org/10.1103/PhysRevB.96.024204)**I. INTRODUCTION**

Multiferroic (MF) materials with strongly coupled ferroelectricity and magnetism is an intriguing challenge nowadays [1–6]. Among various MF materials the doped magnetic ferroelectrics (DMFE) attract a lot of attention since these materials demonstrate the existence of electric polarization and magnetization at room temperatures [7–15]. DMFEs are fabricated by doping of ferroelectrics (FE) with magnetic impurities. Transition metal (TM)-doped BaTiO<sub>3</sub> (BTO) is the most studied material in this family. While both order parameters are simultaneously nonzero in DMFE, the coupling between them (magnetoelectric effect) is very weak and not enough studied [16–18]. Mostly the magnetoelectric (ME) effect in DMFE is related to spin-orbit interaction leading to influence of electric polarization on the material magnetic properties.

In the case of BTO the room temperature ferroelectricity is the internal property of the material. Magnetization appears due to artificially introduced magnetic impurities [7–15]. Several mechanisms of coupling between magnetic impurities are known [19]. At high doping the adjacent magnetic moments directly interact with each other due to electron wave function overlap. This interaction is usually antiferromagnetic. At low impurities concentration (<10%) the direct coupling is not possible. However, the room temperature ferromagnetic (FM) ordering is observed in this limit. The reason for FM interaction between the impurities in this case is shallow donor electrons which inevitably present due to defects such as oxygen vacancies. Donor electrons have weakly localized wave function spanning over several lattice periods. Donor electrons interact with impurities forming a so-called bound magnetic polaron (BMP) in which all magnetic moments are codirected. The polaron size essentially exceeds the interatomic distance. Interaction of the polarons leads to the formation of long-range magnetic order in the system. Due to the large BMP size the critical concentration of defects and magnetic impurities at which FM ordering appears can be rather low. BMPs and their interaction are well understood in doped magnetic semiconductors [19–23].

In the present work we propose a model of magnetoelectric (ME) coupling in DMFE. The idea behind this model is based on the fact that shallow donor electrons interact not only with

magnetic impurities but also with phonons, forming not just magnetic polarons but electromagnetic ones. Magnetic and orbital degrees of freedom are strongly coupled in such a polaron. In contrast to the most magnetoelectric effects based on the spin-orbit interaction, we consider here the ME coupling occurring purely due to the Coulomb interaction. Note that Coulomb-based ME effects were considered recently in a number of other systems [24–28].

The size of the magnetic polaron is defined by the wave function of a donor electron. In its turn the size of the donor electron wave function is defined by electron-phonon interaction and depends on the dielectric properties of the FE matrix [29–32]. It is well known that the dielectric constant of FEs strongly depends on temperature and applied electric field. This opens a way to control magnetic polarons with electric field or temperature. Finally, the magnetization of the whole sample becomes dependent on the external parameters. In the present work we study this mechanism of ME coupling. In particular, we study the magnetic phase diagram of DMFE and show that one can control magnetization with the electric field in such a system.

In DMFEs based on FEs with a high dielectric constant this effect is negligible, which is consistent with the observed weak ME effect in doped BTO. A good FE matrix would be Hf<sub>0.5</sub>Zr<sub>0.5</sub>O<sub>2</sub> [33–35], which has a low dielectric constant ( $\epsilon < 50$ ) strongly dependent on applied electric field. Currently there are no data on Hf<sub>0.5</sub>Zr<sub>0.5</sub>O<sub>2</sub> doped with magnetic impurities. Another magnetic FE with low dielectric constant is (Li,TM) codoped zinc oxide [36–39]. The ME effect in this material can be also strong.

The paper is organized as follows. We present the model in Sec. II. Properties of single magnetic and electric polarons are discussed in Sec. III. Mechanisms of interaction of BMPs are considered in Sec. IV. The magnetic phase diagram of DMFE and ME effects in a number of systems are presented in Sec. V.

**II. THE MODEL**

As we mentioned in the Introduction, the long-range magnetic order in DMFE appears due to interaction of BMPs formed by shallow donor electrons and magnetic impurities. To understand the magnetic properties of DMFE we first study the interaction of two BMPs.

Consider FE with magnetic impurities localized at points  $\mathbf{r}_i^i$ . Each impurity has a spin  $S_0$ . The impurities concentration is low (below 20% [19]) and there is no direct interaction between them. There are also defects with positions  $\mathbf{r}_i^d$  in the system. Their concentration is smaller than the concentration of magnetic impurities. Ordinarily, oxygen vacancies serve as such defects. A defect creates a point charge potential ( $\sim e^2/|\mathbf{r} - \mathbf{r}_i^d|$ ). A charge carrier is bound to each of these defects. The carrier spin is  $s_0 = 1/2$ . The carriers (electrons) interact with impurity spins, forming bound magnetic polarons. Consider two neighboring defects. They are described by the Hamiltonian

$$\hat{H} = \hat{H}_e + \hat{H}_{\text{ph}} + \hat{H}_{e-\text{ph}} + \hat{H}_{e-\text{imp}}, \quad (1)$$

where the carrier energy is given by

$$\hat{H}_e = -\frac{\hbar^2}{2m^*} \sum_i \Delta_i - \frac{e^2}{4\pi \epsilon_0 \epsilon} \left( \sum_{i,j} \frac{1}{|\mathbf{r}_i - \mathbf{r}_j^d|} - \frac{1}{|\mathbf{r}_1 - \mathbf{r}_2|} \right). \quad (2)$$

Here  $m^*$  is the effective mass of electrons in the conduction band of the material in the model of rigid lattice,  $\epsilon$  is the static dielectric constant,  $\epsilon_0$  is the vacuum dielectric constant,  $\mathbf{r}_i$  are the carrier coordinates, and the indices  $i$  and  $j$  take values of either 1 or 2.

The interaction between the carriers and impurities is given by the Hamiltonian

$$\hat{H}_{e-\text{imp}} = J_0 \sum_{i=1,2} \sum_j (\hat{s}_i \hat{S}_j) \delta(\mathbf{r}_j^i - \mathbf{r}_i), \quad (3)$$

where  $\hat{s}_i$  and  $\hat{S}_j$  are the electron and impurity spin operators, respectively. The impurity spin  $S_0$  is usually much larger than one-half.  $J_0$  is the interaction constant. Interaction with magnetic impurities leads to formation of a magnetic polaron.

The terms  $\hat{H}_{\text{ph}}$  and  $\hat{H}_{e-\text{ph}}$  in Eq. (1) are the Hamiltonians of phonons and electron-phonon interaction, respectively [29]. We assume that the carrier interacts mostly with longitudinal optical phonons. Generally, coupling to acoustical phonons and piezoelectric interaction can be taken into account. We neglect them for simplicity, since they are usually weaker than interaction with optical phonons and do not lead to any qualitative changes. The electron-phonon coupling leads to formation of an electric polaron. We will use results of electric polaron theory to describe the electron wave function [29]. The whole system of electrons, magnetic impurities, and phonons is an electromagnetic bound polaron.

### Dielectric properties of FEs

Below we will show that dielectric properties of the FE matrix play crucial role in formation of the magnetic state of DMFE. Therefore, we need to introduce some model of dielectric susceptibility for considered FEs. For simplicity we assume that the dielectric properties of the FE matrix are isotropic. We introduce the dependence of the dielectric permittivity on applied electric field below the Curie temperature:

$$\epsilon^\pm(E) = \epsilon_{\text{min}}^E + \frac{\Delta \epsilon^E}{1 + (E \mp E_s)^2 / \Delta E_s^2}. \quad (4)$$

The superscripts “+” and “−” correspond to the upper and the lower hysteresis branch, respectively,  $E_s$  is the electric field at which the electrical polarization switching occurs, and  $\Delta E_s$  is the width of the switching region.  $\epsilon_{\text{min}}^E$  and  $\Delta \epsilon^E$  define the minimum dielectric constant and its variation with electric field. Equation (4) captures the basic features of dielectric constant behavior. The permittivity has two branches corresponding to two polarization states. In the vicinity of the switching field,  $E_s$  the dielectric permittivity, and  $\epsilon$  has a peak.

Not much data are currently available on the voltage dependencies of  $\epsilon(E)$  for FEs with low dielectric constants. The dielectric constant of  $\text{Hf}_{0.5}\text{Zr}_{0.5}\text{O}_2$  can be described using the following parameters:  $\epsilon_{\text{min}}^E = 30$ ,  $\Delta \epsilon^E = 15$ ,  $E_s = 0.1$  V/nm,  $\Delta E_s = 0.1$  V/nm.

We model the temperature dependence of the FE dielectric constant using the following formula:

$$\epsilon(T) = \epsilon_{\text{min}}^T + \frac{\Delta \epsilon^T}{\sqrt{(T - T_C^{\text{FE}})^2 + \Delta T^2}}. \quad (5)$$

This function allows us to describe the finite height peak at the FE phase transition temperature  $T = T_C^{\text{FE}}$  as well as the  $1/(T - T_C^{\text{FE}})$  dependence in the vicinity of  $T = T_C^{\text{FE}}$ . For simplicity we neglect different behaviors of the dielectric constant above and below  $T_C^{\text{FE}}$ . This does not lead to any qualitative changes in the properties of the considered system.

### III. SINGLE POLARON PROPERTIES

First, consider a single electron located at a defect and interacting with impurities and phonons. In the models of electric and magnetic polarons the electron wave function is chosen in the form of a spherically symmetric wave function,

$$\Psi = \Psi_0 e^{-r/a_B}, \quad (6)$$

where  $a_B$  is the decay length,  $|\Psi_0|^2 = 1/(\pi a_B^3)$ .

#### A. Bound magnetic polaron

First, consider the interaction of a bound electron with impurities leading to formation of a magnetic polaron. Properties of a single magnetic polaron were investigated in the past [19,20,22,40]. Let us calculate the average electron-impurities interaction energy  $\langle \hat{H}_{e-\text{imp}}^s \rangle$  (where the superscript  $s$  indicates that we consider a single polaron) for a given  $a_B$ . Following Ref. [23], we average the magnetic energy over the spatial coordinates

$$\hat{H}_{e-\text{imp}}^s = - \sum_i J_0 (\hat{s}_i) |\Psi(\mathbf{r}_i^i)|^2. \quad (7)$$

The strongest interaction between electron and impurities appears inside the sphere of radius  $r_p$

$$r_p = \frac{a_B}{2} \ln \left( \frac{J}{k_B T} \right), \quad (8)$$

where  $J = S_0 J_0 |\Psi_0|^2 / 2$ ,  $k_B$  is the Boltzmann constant, and  $T$  is the temperature. We assume that  $r_p > a_B$  ( $J > 6k_B T$ ), only in this case magnetic percolation can appear prior to electric percolation (insulator metal transition). The number of impurities within the sphere is  $N_p = 4\pi r_p^3 n_i / 3$ , where  $n_i$  is the impurities concentration.

We assume that the number of impurities within the radius  $r_p$  is big enough. The total spin of impurities relaxes much slower than the spin of the charge carrier. We can introduce the “classical” exchange field (measured in units of energy) acting on the electron magnetic moment:

$$\begin{aligned} \mathbf{B} &= J_0 \left\langle \sum_i |\Psi(\mathbf{r}_i^i)|^2 \hat{\mathbf{S}}_i \right\rangle \approx J_0 \left\langle \sum_{r_i^i < r_p} |\Psi(\mathbf{r}_i^i)|^2 \hat{\mathbf{S}}_i \right\rangle \\ &\approx 2J \left\langle \sum_{r_i^i < r_p} \hat{\mathbf{S}}_i \right\rangle / S_0. \end{aligned} \quad (9)$$

The maximum value of the field is  $B_{\max} \approx 2N_p J$ . Note than in the absence of an electron the impurities spins are independent and the average field value is zero. Field fluctuations are given by  $\sqrt{\langle B^2 \rangle} \approx B_{\max} / \sqrt{N_p}$ .

Equation (7) can be rewritten as follows:

$$\hat{H}_{e-\text{imp}}^s = -(\hat{\mathbf{S}}\mathbf{B}). \quad (10)$$

This Hamiltonian has two nondegenerate eigenstates. For  $J > k_B T$  the average magnitude of the impurities field  $\sqrt{\langle B^2 \rangle} \gg k_B T$ , meaning that even in the case of independent impurities the electron spin should be correlated with the instant meaning of the average field  $\mathbf{B}$ , and  $\langle \hat{\mathbf{S}} \rangle = (1/2)(\mathbf{B}/B)$ . For the energy averaged over the electron spin states we find

$$H_{e-\text{imp}}^s = \langle \hat{H}_{e-\text{imp}}^s \rangle = -B/2. \quad (11)$$

Now we determine the field  $B$  by taking into account the interaction of electron and impurities. This interaction does not lead to the appearance of average  $\mathbf{B}$ . The average absolute value (fluctuations) of  $B = \sqrt{\langle B^2 \rangle}$  is nonzero and is defined by the competition of entropy and internal energy. To find the average  $B$ , consider the states of the system close to the state with full polarization of impurities (within sphere  $r < r_p$ ). The fully polarized state means that all the impurity spins have the same and maximum projection on a certain axis. There is only one such state, but it has the lowest energy. If one reduces the total impurities spin by 1, the energy increases by  $J/S_0$ . At the same time the number of states with reduced spin is  $N_p$ . If  $\ln(N_p) \gg J/(S_0 k_B T)$ , the entropy is the stronger factor than internal energy. In this case the donor electron cannot couple spins of impurities and they are almost independent. In this limit  $H_{e-\text{imp}}^s \approx -B_{\max}/(2\sqrt{N_p})$ . This corresponds to the fluctuation regime of BMP. In the opposite limit,  $\ln(N_p) < J/(S_0 k_B T)$ , the internal energy is dominant. In this case all impurities spins are correlated due to interaction with the electron and  $H_{e-\text{imp}}^s = -B_{\max}/2$ . For  $J = 12k_B T$  (which is in agreement with our requirement  $J_0 > 6k_B T$  and corresponds to  $r_p \approx 1.25 a_B$ ) and  $S_0 = 5/2$  we find  $\ln(N_p) < 4.8$  and  $N_p < 120$ . This estimate is reasonable and the number of impurities in BMP is always within this range [19]. In our work we consider the case of well-correlated BMP, since only in this limit can one expect strong magnetism.

Since  $N_p \approx a_B^3$  and  $J \approx (a_B^3)^{-1}$  the magnetic energy of BMP is independent of the characteristic size of the wave function,  $a_B$ . Therefore, in this regime the interaction with impurities does not influence the electron spatial distribution.

## B. Electric polaron

In the previous section we have shown that interaction with impurities does not influence the Bohr radius of the bound carrier wave function. Therefore,  $a_B$  is defined by the interaction of the electron with defect charge and with phonons. The problem of the electric polaron was studied in the past [29–32]. There are numerous approaches to this problem. We will follow a variational approach of Ref. [41]. The Hamiltonian of a single electric polaron has the form

$$\hat{H}_p = -\frac{\hbar^2}{2m^*} \Delta - \frac{e^2}{4\pi \epsilon_0 \epsilon r} + \hat{H}_{\text{ph}} + \hat{H}_{e-\text{ph}}. \quad (12)$$

The electron wave function is given in Eq. (6). The wave function of phonons is given in Ref. [41]. The radius of the electric polaron  $a_B$  is defined by the minimization of average energy  $\langle \hat{H}_p \rangle$  with respect to  $a_B$ . In the case of strong coupling between the carrier and phonons the Bohr radius is given by [41]

$$(a_B)^{-1} = \frac{m^* e^2}{16\hbar^2} \left( \frac{11}{\epsilon} + \frac{5}{\epsilon_\infty} \right), \quad (13)$$

where  $\epsilon_\infty$  is the optical dielectric constant.

In FE materials the static dielectric constant  $\epsilon$  depends on temperature  $T$  and external electric field  $E$ . Therefore one can control the donor electron wave function size  $a_B$  with an external electric field or by varying temperature.

For materials with a large static dielectric constant  $\epsilon \approx 1000$  (as in BTO, for example) the Bohr radius becomes independent of  $\epsilon$  [ $a_B = 16\hbar^2 \epsilon_\infty / (5m^* e^2)$ ]. In this case variation of  $\epsilon$  with temperature or electric field does not influence the polaron size.

In a number of FEs the static dielectric constant is of the same order as the optical one. For example, in  $\text{Hf}_{0.5}\text{Zr}_{0.5}\text{O}_2$  the static dielectric constant is about 30 while the optical one is about 4.5. (There is no experimental data on  $\epsilon_\infty$  in  $\text{Hf}_{0.5}\text{Zr}_{0.5}\text{O}_2$ ; therefore we use data on  $\text{HfO}_2$  and  $\text{ZrO}_2$  for estimates.) The static dielectric constant of this material depends on the applied electric field [35]. According to Eq. (4), the FE dielectric constant has a peak in the vicinity of the switching field. The polaron radius grows with  $\epsilon$ . Thus,  $a_B(E)$  has also a peak in the vicinity of the switching field  $E_s$ . Variation of  $\epsilon$  with the field in  $\text{Hf}_{0.5}\text{Zr}_{0.5}\text{O}_2$  is about 50% ( $\epsilon_{\min}^E = 30$ ,  $\Delta \epsilon^E = 15$ ). This leads to 10% changes in the polaron radius.

In Li-doped ZnO oxide the static dielectric constant strongly depends on temperature and is not very large. FE properties strongly depend on Li concentration. The FE phase transition in these materials is usually above room temperature [42–45]. In the vicinity of the FE Curie temperature the static dielectric constant varies from 5 to 60. Such a strong growth of the dielectric constant can increase the polaron radius twice.

## IV. INTERACTION OF TWO ELECTROMAGNETIC POLARONS

In this section we consider the magnetic interaction of two electromagnetic polarons in DMFE. We introduce here magnetic moments of these polarons. They have directions  $\mathbf{m}_{1,2}$ . Since there is a large number of impurities in each polaron

we can treat these quantities as classical vectors. The distance  $R = |\mathbf{r}_1^d - \mathbf{r}_2^d|$  between these two polarons exceeds  $2a_B$  and  $2r_p$ . In this case the interpolaron magnetic interaction is weak compared to the magnetic energy of a single polaron. There are three mechanisms of magnetic coupling between polarons: (1) exchange due to the Coulomb interaction in the Hamiltonian Eq. (2) (Heitler-London interaction); (2) magnetic coupling due to the kinetic energy term in the Hamiltonian Eq. (2) (superexchange); and (3) magnetic coupling mediated by impurities, Eq. (3).

### A. Heitler-London interaction between polarons

Consider the Hamiltonian in Eq. (2). If two defects are far away from each other the Hamiltonian can be split into a zero-order Hamiltonian of two noninteracting carriers:

$$\hat{H}_e^{(0)} = -\frac{\hbar^2}{2m^*} \sum_i \Delta_i - \frac{e^2}{4\pi \varepsilon_0 \varepsilon} \sum_i \frac{1}{|\mathbf{r}_i - \mathbf{r}_i^d|} \quad (14)$$

and the perturbation term

$$\hat{H}_e^{(1)} = -\frac{e^2}{4\pi \varepsilon_0 \varepsilon} \left( \frac{1}{|\mathbf{r}_1 - \mathbf{r}_2^d|} + \frac{1}{|\mathbf{r}_2 - \mathbf{r}_1^d|} - \frac{1}{|\mathbf{r}_1 - \mathbf{r}_2|} \right). \quad (15)$$

The wave functions of noninteracting electrons are denoted as  $\Psi_{1,2}$ . In the first-order perturbation theory the Hamiltonian in Eq. (15) produces the spin-dependent interaction between carriers:

$$\hat{H}^{\text{HL}} = 4H^{\text{HL}}(\hat{\mathbf{s}}_1 \hat{\mathbf{s}}_2) = H^{\text{HL}} \cos(\theta). \quad (16)$$

Here we introduce the angle  $\theta$  between magnetic moments of polarons. Since the polaron magnetic moment is large we can treat it as a classical value. As was shown in the previous section, the average spin of the electron is codirected with a corresponding polaron magnetic moment. The exact formula for the exchange constant  $H^{\text{HL}}$  is given elsewhere [46]. The only important thing for us is that it exponentially decays with the distance between the donor centers  $R$  as  $\exp(-2R/a_B)$  and is inversely proportional to  $\varepsilon$ . Thus, we can write

$$H^{\text{HL}} = H_0^{\text{HL}} \frac{e^{-2R/a_B}}{\varepsilon}. \quad (17)$$

Generally, the constant  $H_0^{\text{HL}}$  can be found numerically for wave functions given by Eq. (6).

### B. Superexchange

Magnetic interaction between two electrons appears also due to virtual hopping of electrons between defect sites, so-called superexchange. The coupling appears in the second-order perturbation theory with respect to the hopping matrix elements,  $t = \langle \Psi_1 \Psi_1 | \hat{H}_e | \Psi_1 \Psi_2 \rangle$ . Effective Hamiltonian describing the superexchange is given by [46]

$$\hat{H}^{\text{se}} = \frac{4t^2}{U} (\hat{\mathbf{s}}_1 \hat{\mathbf{s}}_2). \quad (18)$$

Here  $U$  is the on-site repulsion of electrons calculating as  $U = \langle \Psi_1 \Psi_1 | \hat{H}_e | \Psi_1 \Psi_1 \rangle$ . We assume that  $U$  is mostly determined by the Coulomb interaction between two electrons situated at the same site.  $U$  is inversely proportional to the size of the Bohr radius and the system dielectric constant,

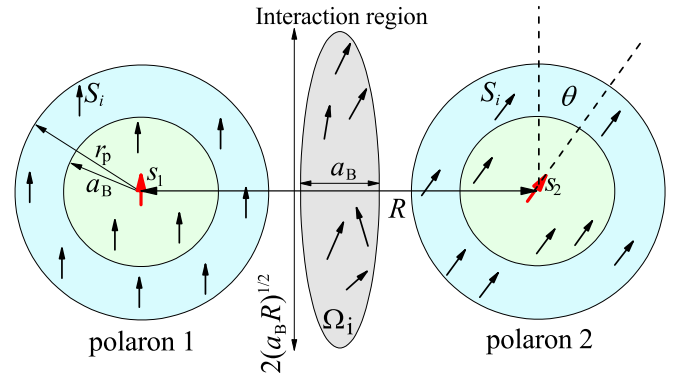


FIG. 1. Two electromagnetic polarons in DMFE separated by a distance  $R$ . The red arrows show the direction of the electrons' average magnetic moments. The angle between magnetic moments of two such electrons is  $\theta$ . The electron wave function characteristic size is  $a_B$ . Black arrows show magnetic moments of impurities in DMFE. Within the magnetic polaron radius  $r_p$  they are codirected with average impurity magnetic moment. In the central area between the polarons there is a lens-shaped interaction region  $\Omega_i$ . Impurities spins in this region are not fully polarized by donor electrons but correlated with them, leading to interaction between the carriers. The width of the interaction region is about  $a_B$ . The lateral size of the region is about  $2\sqrt{R a_B}$ .

$U \approx [1/(\varepsilon a_B)]$ . The hopping matrix element decreases with increasing distance between the defects,  $t^2 \approx \exp(-2R/a_B)$ . Finally, we arrive at the following expression for the interaction energy

$$\begin{aligned} \hat{H}^{\text{se}} &= 4H_0^{\text{se}} a_B \varepsilon e^{-2R/a_B} (\hat{\mathbf{s}}_1 \hat{\mathbf{s}}_2) \\ &= H_0^{\text{se}} a_B \varepsilon e^{-2R/a_B} \cos(\theta) = H^{\text{se}} \cos(\theta). \end{aligned} \quad (19)$$

### C. Impurities-mediated interaction

Consider the situation where the distance between polarons  $R$  exceeds the single polaron size  $r_p$  (see Fig. 1). Beyond the polaron radius  $r_p$  the interaction between the electron and impurities is much weaker than inside the polaron. In the central region between two polarons impurities interact with both electrons, leading to magnetic interaction between carriers (see Fig. 1). We will follow the simplified approach of Ref. [23] to calculate this coupling. According to Ref. [23] the main contribution to the interpolaron interaction is given by lens-shaped region with lateral size  $\sqrt{R a_B}$  and width  $a_B$ . We assume that interaction of the electron with impurities in this region is independent of impurity position. The magnetic energy of this region is given by

$$\hat{H}_{e-\text{imp}}^{\text{p-p}} = 2J e^{-R/a_B} (\hat{\mathbf{s}}_1 + \hat{\mathbf{s}}_2) \sum_{j \in \Omega_i} \hat{\mathbf{S}}_j / S_0, \quad (20)$$

where summation is over the region of interaction  $\Omega_i$ . The number of impurities inside the interaction region can be estimated as  $N_i = \pi a_B^2 R n_i$ . By treating the total polaron spins as classical magnetic moments we obtain

$$\hat{H}_{e-\text{imp}}^{\text{p-p}} = 2J e^{-R/a_B} \cos(\theta/2) \sum_{j \in \Omega_i} \hat{\mathbf{S}}_j^{(z)} / S_0, \quad (21)$$

where  $\theta$  is the angle between the average magnetic moments of polarons. We assume that both polarons are similar and have the same magnetic moment.  $\hat{\mathbf{S}}_j^{(z)}$  is the projection of the impurity spin on the direction  $\mathbf{m}_1 + \mathbf{m}_2$ . The interaction of donor electron and impurities in the region  $\Omega_i$  is weak. Therefore, the average magnetic moment created by this interaction is defined as  $\langle \sum_{j \in \Omega_i} \hat{\mathbf{S}}_j^{(z)} \rangle \approx 2N_i S_0 J e^{-R/a_B} \cos(\theta/2) / (3k_B T)$ . Introducing this result into Eq. (21), we get the average interaction energy of two polarons

$$H_{e\text{-imp}}^{\text{p-p}} = \frac{4N_i J^2 e^{-2R/a_B} \cos^2(\theta/2)}{3k_B T} = H^{\text{p-p}} [\cos(\theta) + 1]. \quad (22)$$

## V. MAGNETIC PHASE DIAGRAM OF DMFE

The distance at which two polarons can be considered as coupled ( $r_c$ ) is defined by the condition

$$|H^{\text{HL}} + H^{\text{se}} + H^{\text{p-p}}| = k_B T. \quad (23)$$

Note that the Heitler-London coupling,  $H^{\text{HL}} > 0$ , and the superexchange,  $H^{\text{se}} > 0$ , produce antiferromagnetic (AFM) coupling while impurity-mediated coupling is FM,  $H^{\text{p-p}} < 0$ . On one hand the first two interactions decay faster with distance ( $e^{-2R/a_B}$ ) than the third one ( $e^{-R/a_B}$ ). But on the other hand the impurity-mediated interaction depends on concentration  $n_i$  and temperature. It decreases with increase of temperature and reduction of  $n_i$ . Experimental results on DMFE show that in most cases FM order appears at low magnetic impurities concentration [9,11,13,16,17,47], meaning that impurity-mediated coupling dominates. However, AFM order is also reported in DMFEs with low impurities concentration [7].

In the case of  $H_0^{\text{HL}} = H_0^{\text{se}} = 0$ , Eq. (23) for the interaction distance  $r_c$  at given temperature  $T$  turns into

$$k_B T = \frac{S_0 J_0 \sqrt{n_i} r_c e^{-r_c/a_B}}{\sqrt{3\pi} a_B^2}. \quad (24)$$

Approximately one can write

$$r_c \approx a_B \left\{ \ln \left[ \frac{S_0 J_0}{2\pi a_B^3 k_B T} \right] + \frac{1}{2} \ln \left[ a_B^3 n_i \ln \left( \frac{S_0 J_0}{2\pi a_B^3 k_B T} \right) \right] \right\}. \quad (25)$$

According to percolation theory [48], the long-range magnetic order in the system of randomly situated polarons appears approximately at  $r_c n_d^{1/3} = 0.86$ , where  $n_d$  is the defect concentration. Introducing  $r_c$  from this relation into Eq. (23) one can find the ordering temperature. Depending on the sign of the total interaction, the ordering can be either FM or AFM (or superspin-glass state).

First, consider the case when the polaron-polaron interaction is the dominant one and we can neglect the Heitler-London and superexchange contributions. In this case there is only FM-type interaction between the impurities and only the FM/paramagnetic (PM) transition is possible. The transition temperature is given by the equation

$$k_B T = \frac{S_0 J_0 \sqrt{0.86 n_i} \exp \left[ -0.86 / (a_B n_d^{1/3}) \right]}{\sqrt{3\pi} n_d^{1/6} a_B^2}. \quad (26)$$

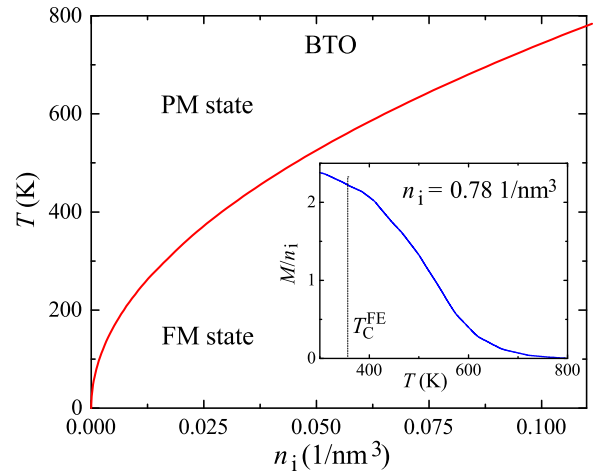


FIG. 2. Approximate magnetic phase transition temperature Eq. (26) as a function of impurities concentration  $n_i$ . The system parameters, which correspond to BTO doped with Fe, are in the text. The inset is the magnetic moment per Fe impurity as a function of temperature for  $n_i = 0.78 \text{ 1/nm}^3$  (5% doping).

Note that according to Eqs. (5), (4), and (13) the Bohr radius,  $a_B(T, E)$ , depends on temperature and external electric field. This makes the PM/FM transition temperature a more complicated function of  $n_i$  and  $n_d$  and makes it dependent on electric field.

The dimensionless magnetization of the DMFE is given by the following equation [23,48]:

$$M(T) = S_0 n_i V_{\text{inf}} [(r_c(T))^3 n_d], \quad (27)$$

where  $V_{\text{inf}}$  is the relative volume of infinite cluster (or probability that an impurity belongs to an infinite cluster) in the site percolation problem. We found the function using the Monte Carlo simulations approach developed in Ref. [49].

### A. BaTiO<sub>3</sub>-based DMFE

Figure 2 shows the magnetic phase diagram of DMFE with the following parameters: The impurities magnetic moment is  $S_0 = 5/2$ . The high-frequency dielectric constant is  $\epsilon_\infty = 5.8$  and the static one is  $\epsilon = 1000$ . We chose such a value of  $m^*$  that  $a_B = 0.45 \text{ nm}$ . This corresponds to the BTO crystal with Fe impurities. Concentration of defects (oxygen vacancies) is about  $0.043 \text{ nm}^{-3}$  (0.27%, lattice period in BTO is about  $0.4 \text{ nm}$ ), and the parameter  $S_0 J_0 = 6 \times 10^4 \text{ K nm}^3$ . At impurities concentration of about 5% this gives spin splitting of the carrier of about  $2.4 \text{ eV}$ . This splitting occurs due to interaction with all impurities within the polaron. We neglect the Heitler-London and superexchange contributions.

The figure shows the magnetic state of the system as a function of impurities concentration and temperature. The system is FM at low temperatures and high impurities concentration and is PM at high temperatures and low concentration of magnetic impurities. The curve in Fig. 2 shows approximate boundary between these two magnetic states. For such a high dielectric constant the Bohr radius  $a_B$  is independent of  $\epsilon$  and the temperature dependence of the dielectric constant does not play any role in magnetic properties of the material.

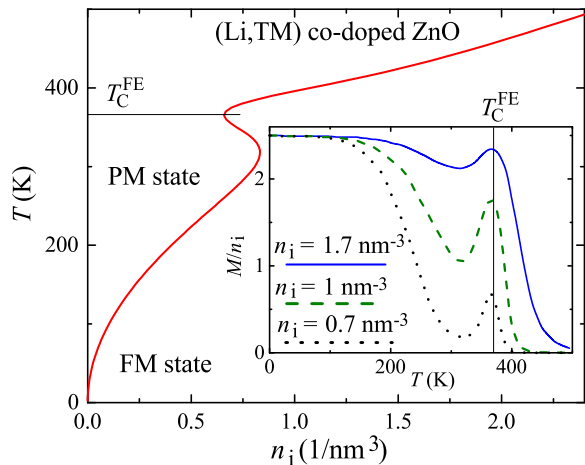


FIG. 3. Magnetic phase diagram of (Li,TM) codoped ZnO. The system parameters are provided in the text. The inset is the magnetic moment per TM impurity as a function of temperature for  $n_i = 1.7 \text{ nm}^{-3}$  (solid blue line),  $1 \text{ nm}^{-3}$  (dashed green line), and  $0.7 \text{ nm}^{-3}$  (dotted black line).

The inset shows magnetization as a function of temperature for impurities concentration  $n_i = 0.78 \text{ 1/nm}^3$  (5% for BTO crystal). The magnetic phase transition appears at  $T \approx 650 \text{ K}$ . This is in agreement with experiment in Ref. [9]. The ferroelectric phase transition in BTO appears at around  $T_C^{\text{FE}} = 360 \text{ K}$ . In this region the dielectric constant has a strong peak. However, because of very large  $\epsilon$  the ME effect is weak and no peculiarities appear in the vicinity of  $T_C^{\text{FE}}$ .

### B. ZnO-based DMFE

(Li,TM) codoped zinc oxide is one of the most studied doped magnetic ferroelectrics [50–52]. Ordinarily, both ferroelectricity and magnetism in these materials appear due to doping. In contrast to “classical” FEs such as BTO, the ZnO-based multiferroics have relatively low dielectric constant. The inevitable defects in doped ZnO materials also provide shallow donor states. Due to the low dielectric constant of the material, the Bohr radius of these states can be temperature dependent.

Magnetism in TM-doped ZnO was theoretically and experimentally studied in numerous works [36–39]. Two distinct cases were recognized when the material is either diluted magnetic semiconductor (DMS) or diluted magnetic insulator (DMI) [38]. In the first case carriers are delocalized on the scale of the whole sample and magnetic ordering appears due to Ruderman-Kittel-Kasuya-Yosida interaction. In the second case carriers are strongly localized and the coupling is due to magnetic polarons. We will assume the small concentration of defects and BMP-based coupling.

Dielectric and magnetic properties in ZnO-based materials strongly depend on the dopant type, concentration, and fabrication procedure. Figure 3 shows the magnetic phase diagram of the DMFE with parameters close to (TM, Li) codoped ZnO. The impurities magnetic moment is  $S_0 = 5/2$  and  $S_0 J_0 = 3.3 \times 10^4 \text{ K nm}^3$ , giving a spin splitting of the electron of about 1.7 eV for impurities concentration  $n_i = 1 \text{ nm}^{-3}$ . The high-frequency dielectric constant is  $\epsilon_\infty = 4$  [19]. The static dielectric constant strongly depends on temperature with

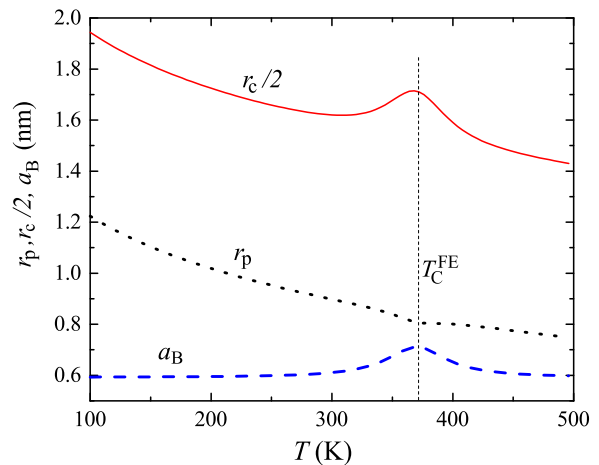


FIG. 4. The Bohr radius  $a_B$ , BMP radius  $r_p$ , and BMP interaction distance  $r_c$  as a function of temperature for DMFE with  $\epsilon$  described by Eq. (4) with  $\epsilon_{\min} = 25$ ,  $\Delta \epsilon = 45$ ,  $T_C^{\text{FE}} = 370 \text{ K}$ , and  $\epsilon_\infty = 4$ . The effective mass is chosen such that the Bohr radius at zero temperature is  $a_B = 0.75 \text{ nm}$ .

$\epsilon_{\min}^T = 25$ ,  $\Delta \epsilon^T = 45$ , and the ferroelectric Curie temperature  $T_C^{\text{FE}} = 370 \text{ K}$  [53]. We chose  $m^*$  such that  $a_B = 0.75 \text{ nm}$  at zero temperature [19]. Concentration of defects (oxygen vacancies) is about  $0.02 \text{ nm}^{-3}$  ( $\sim 0.1\%$ ). We neglect Heitler-London and superexchange contributions.

The magnetic phase transition curve has a peculiarity in the vicinity of the FE phase transition temperature  $T_C^{\text{FE}} = 370 \text{ K}$ . The peculiarity is related to nonmonotonic behavior of the BMP coupling radius  $r_c$  in the vicinity of  $T_C^{\text{FE}}$  (see Fig. 4). Since the static dielectric constant is comparable to the optical one and it has a peak as a function of temperature at  $T = T_C^{\text{FE}}$ , the Bohr radius also has a peak in this region. Increasing  $a_B$  leads to the increase of BMP interaction distance  $r_c$  and enhancement of magnetic properties. Note that while the Bohr radius  $a_B$  and interaction distance  $r_c$  have a peak in the vicinity of the FE phase transition, the BMP radius  $r_p$  has a minimum value (at least for given parameters).

The inset in Fig. 3 shows magnetization of DMFE as a function of temperature for several concentrations of TM impurities. Magnetization also has a peak at  $T = T_C^{\text{FE}}$ . Such a peak is the consequence of coupling between electric and magnetic subsystems in this material and can be considered as a magnetoelectric effect.

In Refs. [51] and [53] the temperature dependence of (Li,TM) co-doped ZnO magnetization was studied in the vicinity of the FE phase transition. No peculiarities in magnetization in the vicinity of the FE transition point were observed. Two possible reasons for the absence of magnetoelectric coupling in these particular samples exist. The first one is that samples studied in Ref. [51] are nanorods of (Li,Co) codoped ZnO with very large surface/volume ratio. The origin of magnetism in such structures is also under question. On one hand the conductivity of these samples is small, meaning that the material is DMI with possible BMP-based magnetism. On the other hand, the magnetism can be related to surface effects, as often happens in nanoscale metal oxides [54,55]. The second possible reason is that the model

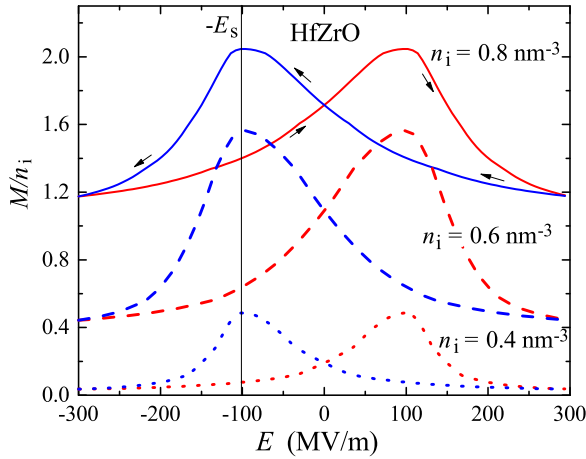


FIG. 5. Dimensionless magnetic moment per magnetic impurity (maximum moment is  $S_0 = 5/2$ ) as a function of applied electric field  $E$  for  $n_i = 0.8 \text{ nm}^{-3}$  (solid lines),  $0.6 \text{ nm}^{-3}$  (dashed lines), and  $0.4 \text{ nm}^{-3}$  (dotted lines). Arrows show the hysteresis bypass direction.

of the electric polaron described in Sec. III B is not applicable to this particular material. Ferroelectricity in this material is related to Li doping and oxygen vacancies [51]. Electric dipoles in this material are inhomogeneously spread across the sample. Therefore, the low-frequency dielectric constant related to these dipoles should be also rather inhomogeneous. Inhomogeneity of the dielectric constant probably appears at the same spatial scale as the distance between magnetic polarons in the system. Therefore, electric dipoles responsible for ferroelectricity and the static dielectric constant do not influence the polaron size.

### C. $\text{Hf}_x\text{Zr}_{1-x}\text{O}_2$ -based DMFE

Another FE family with low dielectric constant is materials based on  $\text{HfO}_2$ . Doping of Hf oxide with various elements leads to the appearance of FE properties (spontaneous electric polarization, hysteresis loop, electric-field-dependent dielectric constant) [33–35]. In the present work we discuss  $\text{Hf}_{0.5}\text{Zr}_{0.5}\text{O}_2$  FE [35]. This material is homogeneous, in contrast to FEs based on weakly doped zinc oxide. This allows us to expect that variation of dielectric constant in this material leads to variation of polaron size. The source of carriers in this material is also oxygen vacancies. No data is available on magnetic doping of this material.

The dielectric constant of  $\text{Hf}_{0.5}\text{Zr}_{0.5}\text{O}_2$  depends on the external electric field. Therefore, one can control the magnetic properties of  $\text{Hf}_{0.5}\text{Zr}_{0.5}\text{O}_2$  doped with magnetic impurities using an electric field. Figure 5 shows the dependence of magnetization of DMFE on external electric field at room temperature and for different impurity concentrations. Other parameters are chosen as follows: The Bohr radius at zero electric field is  $0.5 \text{ nm}$ . The impurities magnetic moment is  $S_0 = 5/2$  and  $S_0 J_0 = 3.3 \times 10^4 \text{ K nm}^3$ , giving the spin splitting of the electron of about  $1.1 \text{ eV}$  for impurities concentration  $n_i = 1 \text{ nm}^{-3}$ . The defects concentration is  $n_d = 0.05 \text{ nm}^{-3}$  ( $\sim 0.6\%$  in the case of  $\text{Hf}_{0.5}\text{Zr}_{0.5}\text{O}_2$ , which has a lattice constant of  $0.5 \text{ nm}$ ). The optical dielectric constant  $\varepsilon_\infty = 4.5$ . The static dielectric constant as a function of electric field is given by

Eq. (4) with  $\varepsilon_{\min}^E = 30$ ,  $\Delta \varepsilon^E = 15$ ,  $E_s = 100 \text{ MV/m}$ , and a switching region width  $\Delta E_s = E_s$  [35]. The Heitler-London and superexchange contributions are neglected.

The static dielectric constant depends on the electric field, leading to electric field dependence of magnetization in the system (ME effect).  $\varepsilon$  demonstrates hysteresis behavior causing hysteresis of magnetization as a function of electric field  $E$ . The dielectric constant reaches its maximum at the switching field  $\pm E_s$ . According to Eq. (25), the BMP interaction distance grows with  $\varepsilon$ . Therefore, the magnetization has peaks at  $E = \pm E_s$ . While interaction distance variation is not large (about 10%) the magnetization variation is significant.

### D. Influence of Heitler-London and superexchange contributions

Since the Heitler-London and superexchange interactions are antiferromagnetic ones, they compete with the BMP-based coupling. These interactions decay faster with distance between defects than the impurities-mediated magnetic coupling, but they do not depend on concentration  $n_i$  and temperature. Therefore, at low impurities concentration and high temperature, antiferromagnetic interactions can dominate, leading to antiferromagnetic (or spin-glass) ordering. At a temperature-independent dielectric constant the AFM ordering temperature can be found as follows:

$$T^{\text{AFM}} = \frac{H^{\text{HL}} + H^{\text{se}} \pm \sqrt{(H^{\text{HL}} + H^{\text{se}})^2 + 4\tilde{H}^{\text{p-p}}}}{2}, \quad (28)$$

where  $\tilde{H}^{\text{p-p}} = -H^{\text{p-p}} k_B T$ . Solutions exist only if  $H^{\text{HL}} + H^{\text{se}} > 2\sqrt{H^{\text{p-p}} k_B T}$ . This condition is always satisfied at low enough impurities concentration. Competition between AFM and FM interactions in DMS was considered in Ref. [22].

Figure 6 shows a magnetic phase diagram of DMFE with significant contribution of the Heitler-London and superexchange interactions. The following parameters are used:  $S_0 = 5/2$ ,  $S_0 J_0 = 4 \times 10^4 \text{ K/nm}^3$ ,  $n_d = 0.02 \text{ nm}^{-3}$ ,  $m^*$  is chosen such that the Bohr radius away from  $T_C^{\text{FE}}$  is about  $0.75 \text{ nm}$ ,  $\varepsilon_\infty = 4$ ,  $\varepsilon_{\min}^T = 25$ ,  $\Delta \varepsilon^T = 35$ ,  $\Delta T = 20 \text{ K}$ ,  $T_C^{\text{FE}} = 370 \text{ K}$ ,  $H_0^{\text{HL}} = 3.5 \times 10^7 \text{ K}$  (main graph),  $H_0^{\text{se}} = 5 \times 10^3 \text{ K/nm}$  (red curves),  $10 \times 10^3 \text{ K/nm}$  (green curves), and  $15 \times 10^3 \text{ K/nm}$  (blue curves). In the inset we use  $H_0^{\text{HL}} = 5 \times 10^6 \text{ K}$ ,  $H_0^{\text{se}} = 3 \times 10^3 \text{ K/nm}$ .

In contrast to the previously considered cases, the region of AFM ordering appears at finite  $H^{\text{HL}}$  and/or  $H^{\text{se}}$ ; the FM/PM boundary also changes. The region of AFM ordering exists only at low impurity concentrations, since only in this case do AFM interactions overcome the strong impurity-mediated FM coupling. The main figure shows the case where direct interactions ( $H^{\text{HL}}$  and  $H^{\text{se}}$ ) are strong and induce AFM ordering at high temperatures close to the FE phase transition. Note that Heitler-London interaction decreases with increase of dielectric constant while the superexchange interaction behaves oppositely. Therefore, the behavior of the phase boundaries strongly depends on the ratio between these two contributions. Superexchange mostly influences the region in the vicinity of the FE phase transition. The AFM region grows and the FM region decreases with increasing  $H_0^{\text{se}}$  in the vicinity of  $T_C^{\text{FE}}$ . The Heitler-London interaction influences the phase diagram aside of  $T_C^{\text{FE}}$ , but this influence is mostly quantitative.

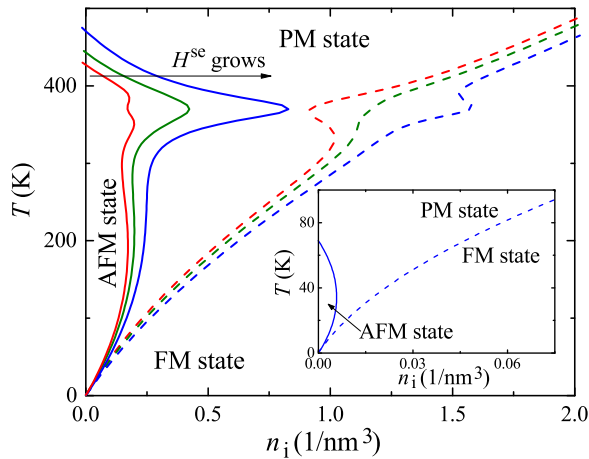


FIG. 6. Magnetic phase diagram of DMFE with strong Heitler-London and superexchange interactions. Solid lines show boundary between PM and AFM states; dashed lines demonstrate PM/FM transition. All curves are plotted for the same  $H_0^{\text{HL}}$ . Red lines correspond to the system with the smallest superexchange contribution, green lines show magnetic phase diagram for a system with intermediate  $H_0^{\text{se}}$ , and blue curves are for the highest  $H_0^{\text{se}}$ . All system parameters are provided in the text. The main figure shows the situation of strong direct coupling leading to AFM ordering in the vicinity of the FE phase transition. The inset shows the case when direct coupling ( $H^{\text{HL}}$  and  $H^{\text{se}}$ ) is weak and induces AFM states only at low temperatures.

The inset shows the case when  $H^{\text{HL}}$  and/or  $H^{\text{se}}$  are relatively small and do not lead to magnetic ordering in the vicinity of the FE phase transition. In this case modifications of the FM/PM boundary are weak. The AFM region exists at low temperatures and low impurities concentration.

## VI. CONCLUSION

In the present work we proposed a coupling mechanism of magnetic and electric degrees of freedom in doped magnetic

ferroelectrics. Magnetic order in DMFE appears due to formation and interaction of BMPs. There are three different contributions to interaction between the magnetic polarons. All these contributions depend on the dielectric constant of the FE matrix. The most significant is the impurities-mediated interaction between polarons. It depends on the radius of the polaron wave function. Due to interaction with phonons, this radius linearly depends on the dielectric constant of the FE matrix. Since the dielectric constant of FEs can be controlled with applied field or varying temperature, one can control the inter-polaron interaction and magnetic state of the whole system. The peculiarity of this magnetoelectric effect is that it does not involve the relativistic spin-orbit coupling and relies only on the Coulomb interaction.

We calculated magnetic phase transition temperatures as a function of impurities concentration and showed that strong temperature dependence of dielectric permittivity in the vicinity of the FE phase transition leads to essential modification of the magnetic phase diagram. We found magnetization as a function of temperature and showed that it has a peak in the vicinity of the FE phase transition. This peak is a consequence of the ME effect appearing in DMFE.

We calculated the magnetization as a function of electric field in DMFE and demonstrated that the magnetic moment of the system can be effectively controlled with applied bias. The magnetization shows hysteresis behavior as a function of electric field. It has two peaks associated with FE polarization switching.

Strong magnetoelectric coupling can appear only in DMFE with low dielectric constant, such as (Li,TM) codoped ZnO or  $\text{Hf}_{0.5}\text{Zr}_{0.5}\text{O}_2$ . TM-doped  $\text{BaTiO}_3$  is not a very promising candidate to observe our effect due to a much larger dielectric constant.

## ACKNOWLEDGMENTS

This research was supported by the NSF under Cooperative Agreement Award No. EEC-1160504 and a NSF PREM Award. O.U. was supported by the Russian Science Foundation (Grant No. 16-12-10340).

- 
- [1] M. Lilienblum, T. Lottermoser, S. Manz, S. M. Selbach, A. Cano, and M. Fiebig, *Nat. Phys.* **11**, 1070 (2015).
  - [2] W. Eerenstein, N. D. Mathur, and J. F. Scott, *Nature (London)* **442**, 759 (2006).
  - [3] R. Ramesh and N. A. Spaldin, *Nat. Mater.* **6**, 21 (2007).
  - [4] H. Zheng, J. Wang, S. E. Lofland, Z. Ma, L. Mohaddes-Ardabili, T. Zhao, L. Salamanca-Riba, S. R. Shinde, S. B. Ogale, F. Bai, D. Viehland, Y. Jia, D. G. Schlom, M. Wuttig, A. Roytburd, and R. Ramesh, *Science* **303**, 661 (2004).
  - [5] M. Bibes and A. Barthélemy, *Nat. Mater.* **7**, 425 (2008).
  - [6] N. Mathur, *Nature (London)* **454**, 591 (2008).
  - [7] A. Barbier, T. Aghavonian, V. Badjcek, C. Mocuta, D. Stanescu, H. Magnan, C. L. Rountree, R. Belkhou, P. Ohresser, and N. Jedrecy, *Phys. Rev. B* **91**, 035417 (2015).
  - [8] L. B. Luo, Y. G. Zhao, H. F. Tian, J. J. Yang, J. Q. Li, J. J. Ding, B. He, S. Q. Wei, and C. Gao, *Phys. Rev. B* **79**, 115210 (2009).
  - [9] B. Xu, K. B. Yin, J. Lin, Y. D. Xia, X. G. Wan, J. Yin, X. J. Bai, J. Du, and Z. G. Liu, *Phys. Rev. B* **79**, 134109 (2009).
  - [10] R. Maier and J. L. Cohn, *J. Appl. Phys.* **92**, 5429 (2002).
  - [11] Y.-H. Lin, J. Yuan, S. Zhang, Y. Zhang, J. Liu, Y. Wang, and C.-W. Nan, *Appl. Phys. Lett.* **95**, 033105 (2009).
  - [12] Y. Shuai, S. Zhou, D. Bürger, H. Reuther, I. Skorupa, V. John, M. Helm, and H. Schmidt, *J. Appl. Phys.* **109**, 084105 (2011).
  - [13] W. Bai, X. J. Meng, T. Lin, L. Tian, C. B. Jing, W. J. Liu, J. H. Ma, J. L. Sun, and J. H. Chu, *J. Appl. Phys.* **106**, 124908 (2009).
  - [14] X. K. Wei, Y. T. Su, Y. Sui, Q. H. Zhang, Y. Yao, C. Q. Jin, and R. C. Yu, *J. Appl. Phys.* **110**, 114112 (2011).
  - [15] Y. Wang, G. Xu, X. Ji, Z. Ren, W. Weng, P. Du, G. Shen, and G. Han, *J. Alloys Compd.* **475**, L25 (2009).
  - [16] M. Kumari, D. G. B. Diestra, R. Katiyar, J. Shah, R. K. Kotnala, and R. Chatterjee, *J. Appl. Phys.* **121**, 034101 (2017).

- [17] X. Ye, Z. Zhou, W. Zhong, D. Hou, H. Cao, C. Au, and Y. Du, *Thin Solid Films* **519**, 2163 (2011).
- [18] J. Shah and R. K. Kotnala, *J. Mater. Chem. A* **1**, 8601 (2013).
- [19] J. M. D. Coey, M. Venkatesan, and C. B. Fitzgerald, *Nat. Mater.* **4**, 173 (2005).
- [20] T. Dietl and J. Spafek, *Phys. Rev. B* **28**, 1548 (1983).
- [21] D. E. Angelescu and R. N. Bhatt, *Phys. Rev. B* **65**, 075211 (2002).
- [22] A. C. Durst, R. N. Bhatt, and P. A. Wolff, *Phys. Rev. B* **65**, 235205 (2002).
- [23] A. Kaminski and S. Das Sarma, *Phys. Rev. Lett.* **88**, 247202 (2002).
- [24] O. G. Udalov, N. M. Chitchev, and I. S. Beloborodov, *J. Phys.: Condens. Matter* **27**, 186001 (2015).
- [25] O. G. Udalov, N. M. Chitchev, and I. S. Beloborodov, *Phys. Rev. B* **92**, 045406 (2015).
- [26] O. G. Udalov and I. S. Beloborodov, *Phys. Rev. B* **95**, 045427 (2017).
- [27] O. G. Udalov and I. S. Beloborodov, *J. Phys.: Condens. Matter* **29**, 175804 (2017).
- [28] O. G. Udalov and I. S. Beloborodov, *J. Phys.: Condens. Matter* **29**, 155801 (2017).
- [29] T. K. Mitra, A. Chatterjee, and S. Mukhopadhyay, *Phys. Rep.* **153**, 91 (1987).
- [30] G. Whitfield and P. M. Platzman, *Phys. Rev. B* **6**, 3987 (1972).
- [31] K. Hattori, *J. Phys. Soc. Jpn.* **38**, 669 (1975).
- [32] M. Engineer and G. Whitfield, *Phys. Rev.* **179**, 869 (1969).
- [33] T. S. Böske, St. Teichert, D. Bräuhäus, J. Müller, U. Schröder, U. Böttger, and T. Mikolajick, *Appl. Phys. Lett.* **99**, 112904 (2011).
- [34] J. Müller, U. Schröder, T. S. Böske, I. Müller, U. Böttger, L. Wilde, J. Sundqvist, M. Lemberger, P. Kücher, T. Mikolajick, and L. Frey, *J. Appl. Phys.* **110**, 114113 (2011).
- [35] J. Müller, T. S. Böske, U. Schröder, S. Mueller, D. Bräuhäus, U. Böttger, L. Frey, and T. Mikolajick, *Nano Lett.* **12**, 4318 (2012).
- [36] F. Pan, C. Song, X. J. Liu, Y. C. Yang, and F. Zeng, *Mater. Sci. Eng., R* **62**, 1 (2008).
- [37] M. Venkatesan, C. B. Fitzgerald, J. G. Lunney, and J. M. D. Coey, *Phys. Rev. Lett.* **93**, 177206 (2004).
- [38] A. J. Behan, A. Mokhtari, H. J. Blythe, D. Score, X.-H. Xu, J. R. Neal, A. M. Fox, and G. A. Gehring, *Phys. Rev. Lett.* **100**, 047206 (2008).
- [39] M. H. F. Sluiter, Y. Kawazoe, P. Sharma, A. Inoue, A. R. Raju, C. Rout, and U. V. Waghmare, *Phys. Rev. Lett.* **94**, 187204 (2005).
- [40] P. A. Wolff, *Semicond. Semimet.* **25**, 413 (1988).
- [41] D. M. Larsen, *Phys. Rev.* **187**, 1147 (1969).
- [42] C. W. Zou, M. Li, H. J. Wanga, M. L. Yin, C. S. Liu, L. P. Guo, D. J. Fu, and T. W. Kang, *Nucl. Instrum. Methods Phys. Res., Sect. B* **267**, 1067 (2009).
- [43] Dhananjay, J. Nagaraju, and S. B. Krupanidhi, *J. Appl. Phys.* **99**, 034105 (2006).
- [44] M. K. Gupta and B. Kumar, *J. Alloys Compd.* **509**, L208 (2011).
- [45] S. U. Awan, S. K. Hasanain, G. H. Jaffari, and Z. Mehmood, *Appl. Phys. Lett.* **104**, 222906 (2014).
- [46] A. Auerbach, *Interacting Electrons and Quantum Magnetism* (Springer-Verlag, New York, 1994).
- [47] J. Lee, Z. Khim, Y. Park, D. Norton, N. Theodoropoulou, A. Hebard, J. Budai, L. Boatner, S. Pearton, and R. Wilson, *Solid-State Electron.* **47**, 2225 (2003).
- [48] B. I. Shklovskii and A. L. Efros, *Electronic Properties of Doped Semiconductors* (Springer-Verlag, Berlin, 1984).
- [49] D. F. Holcomb and J. J. R. Rehr, Jr., *Phys. Rev.* **183**, 773 (1969).
- [50] C. W. Zou, H. J. Wanga, M. L. Yin, M. Li, C. S. Liu, L. P. Guo, D. J. Fu, and T. Kang, *J. Cryst. Growth* **312**, 906 (2010).
- [51] C. W. Zou, L. X. Shao, L. P. Guo, D. J. Fu, and T. W. Kang, *J. Cryst. Growth* **331**, 44 (2011).
- [52] Y.-H. Lin, M. Ying, M. Li, X. Wang, and C.-W. Nan, *Appl. Phys. Lett.* **90**, 222110 (2011).
- [53] F. Pan, X. J. Liu, Y. C. Yang, C. Song, and F. Zeng, *Mater. Sci. Forum* **620–622**, 735 (2009).
- [54] R. Escudero and R. Escamilla, *Solid State Commun.* **151**, 97 (2011).
- [55] A. Sundaresan and C. N. R. Rao, *Nano Today* **4**, 96 (2009).